RESEARCH ARTICLE

WILEY

Dynamic diffusion tensor imaging of spinal cord contusion: A canine model

Changbin Liu[1,2,3,4,5] (ORCID) | Degang Yang[1,2,3,4,5] | Jianjun Li[1,2,3,4,5] | Dapeng Li[1,2,3,4,5] |
Mingliang Yang[1,2,3,4,5] | Wei Sun[1,3,4,5] | Qianru Meng[1,2,3,4,5] | Wenhao Zhang[1,2,3,4,5] |
Chang Cai[1,2,3,4,5] | Liangjie Du[1,2,3,4,5] | Jun Li[1,2,3,4,5] | Feng Gao[1,2,3,4,5] |
Rui Gu[1,3,4,5] | Yutong Feng[1,2,3,4,5] | Xuechao Dong[1,2,3,4,5] | Qi Miao[6] |
Xinghua Yang[7] | Zhentao Zuo[8,9,10]

[1]School of Rehabilitation Medicine, Capital Medical University, Beijing 100068, China

[2]Department of Spinal and Neural Function Reconstruction, China Rehabilitation Research Center, Beijing 100068, China

[3]Center of Neural Injury and Repair, Beijing Institute for Brain Disorders, Beijing 100068, China

[4]China Rehabilitation Science Institute, Beijing 100068, China

[5]Beijing Key Laboratory of Neural Injury and Rehabilitation, Beijing 100068, China

[6]Zibo Shanhang Medical Engineering Co., ltd, Zibo, Shandong 255000, China

[7]School of Public Health, Capital Medical University, 10 Xitoutiao, Youanmen, Beijing 100069, China

[8]State Key Laboratory of Brain and Cognitive Science, Institute of Biophysics, Chinese Academy of Sciences, Beijing, China

[9]The Innovation Center of Excellence on Brain Science, Chinese Academy of Sciences

[10]Sino-Danish College, University of Chinese Academy of Sciences, Beijing 100049, China

Correspondence
Dr Jianjun Li, School of Rehabilitation Medicine, Capital Medical University; Department of Spinal and Neural Function Reconstruction, China Rehabilitation Research Center; Center of Neural Injury and Repair, Beijing Institute for Brain Disorders; Beijing Key Laboratory of Neural Injury and Rehabilitation, No. 10 Jiaomen North Road, Fengtai District, Beijing 100068, China. Email: 13718331416@163.com

Abstract

This study aimed to explore the dynamic diffusion tensor imaging (DTI) of changes in spinal cord contusion using a canine model of injury involving rostral and caudal levels. In this study, a spinal cord contusion model was established in female dogs using a custom-made weight-drop lesion device. DTI was performed on dogs with injured spinal cords (n=7) using a Siemens 3.0T MRI scanner at pre-contusion and at 3 h, 24 h, 6 weeks and 12 weeks post-injury. The tissue sections were stained for immunohistochemical analysis. Canine models of spinal cord contusion were created successfully using the weight-drop lesion device. The fractional anisotropy (FA) value of lesion epicenter decreased, while the apparent diffusion coefficient (ADC), mean diffusivity (MD), and radial diffusivity (RD) values increased, and the extent of the curve was apparent gradually. The site and time affected the DTI parameters significantly in the whole spinal cord, ADC (site, $P < 0.001$ and time, $P = 0.077$, respectively); FA (site, $P < 0.001$ and time, $P = 0.002$, respectively). Immunohistological analysis of GFAP and NF revealed the pathologic changes of reactive astrocytes and axons, as well as the cavity and glial scars occurring during chronic SCI. DTI is a sensitive and noninvasive imaging tool useful to assess edema, hemorrhage, cavity formation, structural damage and reconstruction of axon, and myelin in dogs. The DTI parameters after contusion vary. However, the curves of ADC, MD, and RD were nearly similar and the FA curve was distinct. All the DTI parameters were affected by distance and time.

KEYWORDS

diffusion tensor imaging, dogs, dynamic changes, model, histopathology, RRID: AB_650102, RRID: AB_880202

Significance

This study established a canine model of spinal cord contusion and determined the dynamic changes in DTI parameters of the whole spinal cord post SCI. We further demonstrated that DTI is a sensitive and noninvasive imaging tool to assess edema, hemorrhage, cavity formation, axon and myelin structure damage, and reconstruction in dogs. Although the study is preliminary, our results offered an experimental basis for fundamental and clinical research. Our canine model is translational and facilitates investigation into human spinal cord pathology.

1 | INTRODUCTION

Traumatic spinal cord injury (SCI) is a devastating and debilitating disease with an annual incidence rate ranging between 11.5 and 57.8 cases per million population (Ackery, A., Tator, C., & Krassioukov, 2004). Despite advances in basic and clinical research over the past 20 years, effective strategies to reverse spinal cord injury and functional restoration are still lacking. The prognosis remains poor, with apparent disability and quadriplegia under severe conditions leading to defecation disorders and inability to attend to activities of daily life. Consequently, the patients bring about a heavy economic burden to the society and family (Chiu et al., 2010; Onose et al., 2009). Researchers have developed a number of SCI models, especially in animals in terms of indices including clip compression, weight dropping, balloon compression, hemisection, contusion, and transection and segment resection in an effort to investigate the treatment strategies (Fukuda et al., 2005; Khan & Griebel, 1983; Wang, Huang, He, & Li, 2014).

Currently, models for the studies on SCI are mostly confined to rodents, such as rats and mice. Spinal cord anatomy is relatively small and may lead to further damage, resulting in larger error. Reports suggest that the canine model of SCI resembles human SCI in terms of mechanisms of injury, pathology, outcome, classification, and functional monitoring and represents an ideal translational model for rodent experiments and human clinical trials (Boekhoff et al., 2012; Jeffery et al., 2006). Purdy et al. (2004) described similarities between canine and human spinal cord in terms of imaging. A larger experimental canine model might represent a possible alternative to investigate SCI due to similarities with human anatomy, surgical feasibility, and clinical application. Histopathological analysis is the gold standard of evaluation using the canine model of SCI, edema, hemorrhage, and axonal changes. However, as an invasive technique, histopathological examination has limited application in monitoring the dynamic changes following SCI and clinical treatment (C. Zhao et al., 2016).

Conventional MRI techniques (spin echo, gradient echo, and inversion recovery sequences, with T1-, T2-, or proton density-weighting) have continued to evolve over the past three decades, establishing MRI as the imaging modality of choice for most spinal disorders (Martin et al., 2016). MRI also provides important insights into the severity of SCI, including the presence of spinal cord edema, hemorrhage, and contusion (Kulkarni et al., 1987). However, applications of conventional MRI techniques are limited in developing imaging biomarkers or predicting clinical outcomes because of their limited sensitivity and specificity in detecting the degenerative and regenerative changes occurring within the spinal cord at the microstructural and functional levels (Ellingson, Kurpad, & Schmit, 2008). Diffusion tensor imaging (DTI) facilitates analysis of the changes in tissue architecture and neuronal tract structure in vivo via selective preference for aqueous diffusion (Basser, Mattiello, & LeBihan, 1994). In addition, the severity of injury at the acute stage can also be evaluated (Loy et al., 2007). It provides data underlying the microstructural integrity of the tissue under investigation (Hobert, Stein, Dziallas, Ludwig, & Tipold, 2013; Lee et al., 2011; Patel et al., 2016; Tay, Hyun, & Oh, 2014; Xiangshui et al., 2010). The technique has great significance for the evaluation of SCI model and dynamic quantitative observation of SCI. The major DTI metrics that are routinely measured include apparent diffusion coefficient (ADC), fractional anisotropy (FA), mean diffusivity (MD), and radial diffusivity (RD; Leong et al., 2015). To our knowledge, the dynamic changes involving DTI parameters of longitudinal spinal cord, which involves the lesion epicenter and both rostral and caudal levels post SCI in dogs, are yet to be elucidated.

Accordingly, the aim of the research was to establish a canine model of spinal cord contusion and to explore the dynamic changes in DTI parameters of the whole spinal cord, from the lesion epicenter to rostral and caudal levels over an extended duration post SCI. Histopathology and immunohistochemical staining of sections were also conducted to relate changes on DTI to the underlying pathology.

2 | MATERIALS AND METHODS

2.1 | Ethics statement

The Experimental Animal Center of Capital Medical University approved all the animal procedures. The study was conducted according to the ethical rules of Animal Experiments and Experimental Animal Welfare Committee (AEEI-2015-055).

2.2 | Animals

Seven healthy female (10 ± 0.5 kg, 2 ± 0.5 y) beagles (Beijing Marshall Biotechnology Co.) were included in the current study and were allowed access to food and water ad libitum. None of the dogs showed clinical signs of an underlying disorder of the spinal cord with normal spinal cord morphology based on standard MRI protocols under anesthesia. Dogs with the suspected neurological disorder affecting the spinal cord, history of spinal cord disease, or surgery were excluded.

2.3 | Spinal cord injury

The dogs were anesthetized via intraperitoneal administration of 2.5% pentobarbital sodium (Merck) with a dose of 125 mg/kg, and an intramuscular administration of xylazine hydrochloride (Dunhua Shengda Animal Pharmaceutical Co., Ltd.) 0.1 ml/kg. The animals were held on the operating table in the prone position. Retention catheterization
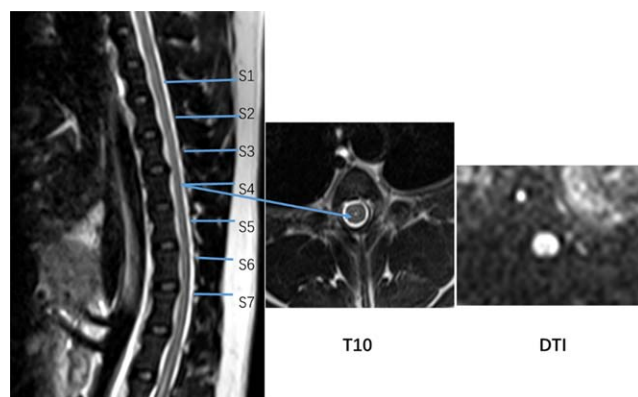
FIGURE 1 The injury epicenter was T10, we defined 7 regions of interest (ROIs) from the epicenter to rostral and caudal level at intervals of 1 cm, and designated as sites 1-7 from rostral to caudal level. [Color figure can be viewed at wileyonlinelibrary.com]

was managed using sterile urethral catheter (8Fr, Zhanjiang Star Enterprise Co., Ltd.). Intraoperative antimicrobials were administered via intravenous injection at the time point of surgical decompression of the spinal cord (cefoxitin sodium; Webb, Ngan, & Fowler, 2010). A rectangular skin area (30 cm × 15 cm) centered on the 10th thoracic vertebra was marked. After conventional betadine and alcohol disinfection, an incision length of 6 cm was made around the midpoint of the T10 spinous process under sterile conditions. The adipose layer and fascia were cut cautiously. The spinous process and the adjacent muscles were bluntly dissected ensuring adequate hemostasis. The T9, T10, and T11 spinous processes and the interspinal ligaments were cut. Vertebral laminae of T10 and part of T9 and T11 were uncovered to expose a 1-cm long spinal cord as described previously (Dong et al., 2016).

In the current study, a new spinal cord contusion impactor was designed, which was appropriate for large animals based on the principle of the MASCIS Impactor Method (Young, 2002; Patent No: ZL 2016 2 0915673.4). The spine of each animal was clamped using a spinous process clip to center the T10 spinal cord under the head of a falling hammer weighing 20 g. We first dropped the hammer until it nearly contacted the spinal dura, followed by calibration of the device. The falling hammer was raised then to a certain height (25 cm) and was released in a free fall to induce the SCI and fishtailing phenomenon. The standard of data (impact velocity, force, displacement, and dwell time) was the same. Immediately following injury, the wounds were irrigated with saline ensuring adequate hemostasis, and the injured spinal cord with a piece of gelatin sponge. The muscle layers were sutured together with a 3-0 absorbable surgical suture. The skin was sutured with a 1-0 surgical suture.

2.4 | Postoperative nursing

Hydrogen peroxide and betadine were used to clean the surgical site and bound using sterile gauze. After the dogs regained consciousness, they were administered orally with pregabalin (25 mg/kg, Pfizer) every day for one week. All the dogs continued to receive sodium chloride injection (25 mL/kg) intravenously for 3 days post-injury. The antibiotic

agent cefoxitin sodium (50 mg/kg) was administered via intramuscular injection daily for 7 days.

All the dogs were fed with enteral nutritional suspension (100 mL/10kg, bid, Nutricia Pharmaceutical Co., Ltd) through 1-week post-injury (WPI) and allowed access to food and water ad libitum. The betadine was smeared on the animals' hips and the waterproof mat in the cages was renewed each day to prevent pressure ulcers. The catheter was extricated upon recovery of the bladder-emptying reflex, typically within 2 to 3 weeks post-injury.

2.5 | MRI

The experiments were performed using Siemens 3.0T Prisma fit MRI scanner (Siemens Magnetom) with a 32 Ch Spinal cord coil. The animals were placed in the supine position under anesthesia during the entire MRI scan with a mixture of pentobarbital sodium and xylazine hydrochloride. Fat-saturated sagittal T2-SPACE sequences were acquired with an in-plane resolution of 0.84 mm × 0.84 mm (TR/TE = 1500/142 ms) with the slice thickness of 0.75 mm and with an ACQ matrix size of 320 × 320. Axial diffusion imaging was based on single-shot EPI sequence using the following parameters: TR/TE of 7300/83 ms, slice thickness of 4 mm with a 0.8 mm gap, in-plane resolution of 1.3 mm × 1.3 mm, 30 directions, b values of 800, NEX = 2, and extra 4 b0 images. The timing of the MRI exams was at precontusion and at 3 h, 24 h, 6 weeks, and 12 weeks post-injury.

2.6 | DTI pre-processing

The centerline of white matter was defined on T2w imaging using the custom software. DTI preprocessing pipeline included: (1) Registration to T2w images, (2) correction for eddy current, and (3) calculation of DTI parameters, FA, ADC, MD, and RD. The injury epicenter was T10, which was defined as 7 regions of interest (ROIs) from the epicenter to rostral and caudal level at intervals of 1 cm, and designated as sites 1-7 from rostral to caudal level. The parameters of the seven sites were analyzed in the study (Figure 1).

2.7 | Histopathology and immunohistochemistry

Following 3 months of post-injury MRI, animals were anesthetized and surgery was performed as described previously. To maintain consistent sampling, each spinal cord was transected at the rostral T9 spinal root and a 3-cm spinal cord segment was immediately dissected and post-fixed in 4% paraformaldehyde (PFA) at 4° C (Patel et al., 2016). The injured spinal cord was transected to about 5 mm segments, respectively, which were juxtaposed with the rostral ends of each cord evenly aligned into plastic cryomolds with paraffin embedding (Rabchevsky, Fugaccia, Sullivan, Blades, & Scheff, 2002). The embedded spinal cords were cut into 3-μm transverse sections, except that two spinal lesions were cut longitudinally. The spinal cord sections were mounted on gelatinized slides and stained with hematoxylin and eosin (HE) for histopathological and morphological observation. Immunohistochemical analysis of the spinal cord lesion was conducted by incubating a few longitudinal and transversal sections overnight at 4° C with primary

TABLE 1 The primary antibodies

Antibodies	Source, host species, cat. #, RRID	Applications	Description of immunogen
NF-H(E-15):sc-22909	Santa Cruz Biotechnology, goat polyclonal, Cat# sc-22909 RRID:AB_650102	Immunohistochemistry (dilution 1:100)	epitope mapping within an internal region of NF-H of human origin
Anti-GFAP antibody (ab53554)	Abcam, goat polyclonal, Cat# ab53554 RRID:AB_880202	Immunohistochemistry (dilution 1:200)	Synthetic peptide corresponding to Human GFAP aa 417-430 (C terminal) (Cysteine residue).

antibodies against NF-H (dilution 1:100, Santa,sc-22909) and mouse monoclonal anti-GFAP (1:200, Abcam,ab53554). After washing with phosphate-buffered saline (PBS) 0.2% for 5 min, the sections were incubated with conjugated secondary antibody immunoCruz™ goat ABC staining system (Santa) for 2 h at room temperature, followed immediately by 1 to 2 drops of permanent mounting medium, and covered with a glass coverslip (Grace et al., 2010; Hu et al., 2010; Xu et al., 2011). Finally, all the sections were imaged with HistoFAXS software (Tissue Gnostics) at a magnification of 20 × (Table 1).

2.8 | Statistical analysis

Statistical analysis was performed with SPSS 21.0 (SPSS Inc.). The normal distribution of the data was tested with the Shapiro-Wilk normality tests. The basal repeated measures analysis of variance was used to analyze the measurement parameters of different time points at the same site. The mixed-effects modeling was used to analyze the related factors on the DTI parameters. The data were expressed as mean ± standard deviation (SD). Values of $P < 0.05$ were considered statistically significant.

3 | RESULTS

3.1 | Spinal cord contusion model

Following impact, the dogs' tails showed rapid convulsions. The bilateral hind limbs appeared flaccid and paralyzed as the effect of anesthesia dissipated. The gait and postural reactions remained scoreless and
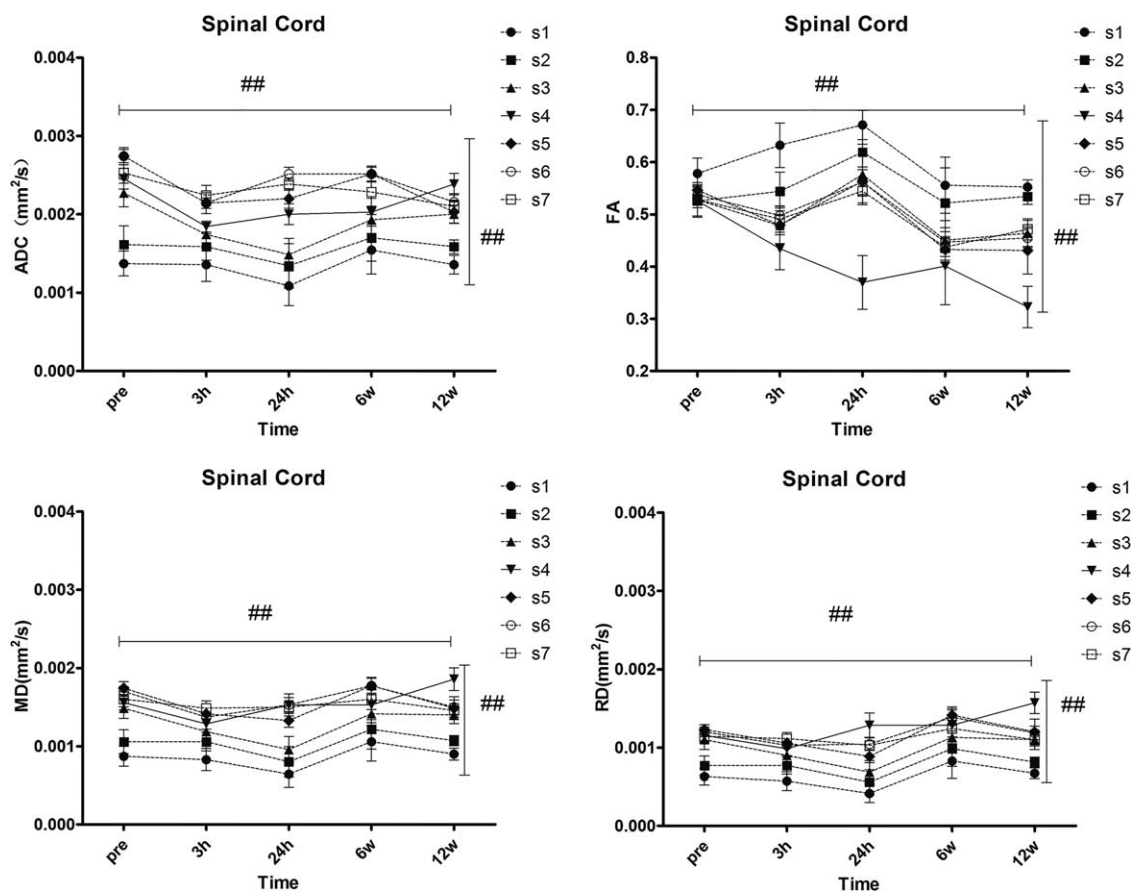

FIGURE 2 Line chart of ADC, FA, MD, and RD values over time at seven sites in the whole spinal cord. An error probability of 0.05 (P) was used as significance level. All the parameters were expressed as mean ± standard deviation (SD). ##, $P < 0.001$. The horizontal capped line suggests a significant effect of time on these parameters. The vertical capped line indicates the significant impact of site location on them

TABLE 2 The description of DTI parameters of all sites over time in the spinal cord

DTI ROI	Pre-SCI	3h	1d	6w	12w	F	P
ADC (10^{-3}mm^2/s)							
Site 1	1.371 ± 0.158	1.355 ± 0.216	1.095 ± 0.251	1.547 ± 0.304	1.364 ± 0.115	74.58	<0.001
Site 2	1.614 ± 0.239	1.582 ± 0.173	1.338 ± 0.284	1.704 ± 0.296	1.586 ± 0.088	127.46	<0.001
Site 3	2.271 ± 0.174	1.743 ± 0.153	1.488 ± 0.207	1.929 ± 0.173	2.000 ± 0.116	387.54	<0.001
Site 4	2.457 ± 0.133	1.843 ± 0.069	2.000 ± 0.133	2.029 ± 0.179	2.386 ± 0.137	5818.96	<0.001
Site 5	2.743 ± 0.109	2.143 ± 0.069	2.200 ± 0.123	2.514 ± 0.103	2.029 ± 0.141	1026.22	<0.001
Site 6	2.743 ± 0.084	2.143 ± 0.134	2.514 ± 0.088	2.514 ± 0.088	2.157 ± 0.107	2057.71	<0.001
Site 7	2.529 ± 0.132	2.243 ± 0.127	2.386 ± 0.080	2.286 ± 0.194	2.100 ± 0.082	1186.31	<0.001
FA							
Site 1	0.578 ± 0.029	0.632 ± 0.042	0.671 ± 0.028	0.556 ± 0.053	0.553 ± 0.013	601.94	<0.001
Site 2	0.525 ± 0.028	0.544 ± 0.036	0.619 ± 0.051	0.522 ± 0.067	0.534 ± 0.015	973.45	<0.001
Site 3	0.528 ± 0.033	0.478 ± 0.034	0.576 ± 0.058	0.450 ± 0.037	0.464 ± 0.025	593.03	<0.001
Site 4	0.526 ± 0.013	0.434 ± 0.040	0.369 ± 0.051	0.401 ± 0.073	0.323 ± 0.039	265.18	<0.001
Site 5	0.546 ± 0.010	0.479 ± 0.018	0.563 ± 0.028	0.433 ± 0.025	0.431 ± 0.045	774.70	<0.001
Site 6	0.538 ± 0.014	0.498 ± 0.017	0.562 ± 0.023	0.447 ± 0.020	0.455 ± 0.018	8199.97	<0.001
Site 7	0.528 ± 0.010	0.491 ± 0.025	0.544 ± 0.022	0.437 ± 0.017	0.471 ± 0.020	2558.99	<0.001
MD (10^{-3}mm^2/s)							
Site 1	0.885 ± 0.125	0.829 ± 0.139	0.646 ± 0.167	1.056 ± 0.243	0.895 ± 0.079	64.29	<0.001
Site 2	1.049 ± 0.155	1.004 ± 0.125	0.807 ± 0.193	1.217 ± 0.250	1.067 ± 0.067	110.48	<0.001
Site 3	1.486 ± 0.129	1.187 ± 0.115	0.959 ± 0.168	1.406 ± 0.160	1.400 ± 0.109	290.71	<0.001
Site 4	1.557 ± 0.094	1.285 ± 0.067	1.529 ± 0.142	1.536 ± 0.191	1.857 ± 0.146	1054.29	<0.001
Site 5	1.743 ± 0.081	1.414 ± 0.040	1.329 ± 0.089	1.771 ± 0.108	1.484 ± 0.148	527.09	<0.001
Site 6	1.700 ± 0.061	1.371 ± 0.068	1.529 ± 0.094	1.771 ± 0.094	1.500 ± 0.092	2422.35	<0.001
Site 7	1.600 ± 0.097	1.486 ± 0.093	1.500 ± 0.065	1.599 ± 0.133	1.457 ± 0.084	1596.05	<0.001
RD (10^{-3}mm^2/s)							
Site 1	0.637 ± 0.104	0.587 ± 0.118	0.410 ± 0.117	0.823 ± 0.224	0.674 ± 0.062	51.38	<0.001
Site 2	0.764 ± 0.118	0.782 ± 0.106	0.561 ± 0.161	0.984 ± 0.228	0.800 ± 0.055	90.48	<0.001
Site 3	1.105 ± 0.121	0.897 ± 0.101	0.675 ± 0.152	1.134 ± 0.153	1.105 ± 0.122	203.33	<0.001
Site 4	1,147 ± 0.087	0.995 ± 0.084	1.285 ± 0.155	1.297 ± 0.209	1.570 ± 0.136	433.43	<0.001
Site 5	1.223 ± 0.068	1.063 ± 0.039	0.885 ± 0.081	1.413 ± 0.106	1.201 ± 0.162	270.97	<0.001
Site 6	1.200 ± 0.061	1.029 ± 0.040	1.041 ± 0.082	1.386 ± 0.096	1.185 ± 0.085	3801.84	<0.001
Site 7	1.143 ± 0.083	1.117 ± 0.075	1.019 ± 0.061	1.238 ± 0.110	1.102 ± 0.079	1394.34	<0.001

The parameters of diffusion tensor imaging (DTI) including apparent diffusion coefficient (ADC), fractional anisotropy (FA), mean diffusivity (MD), and radial diffusivity (RD) at different sites of spinal cord. All the parameters were expressed as mean ± SD, $n = 7$. Site 4 was the epicenter, site 1 was rostral, site 7 was caudal, and they were separated by 1 cm, respectively.

nociception in each limb was one point within 2 days, suggesting successful creation of the model (Dong et al., 2016).

3.2 | DTI

The ADC values at different sites varied significantly at all time points, with lower values closer to the rostral level, and increasing with proximity to the caudal level. The mixed-effects modeling analysis showed that the site location influenced ADC parameters significantly ($P < 0.001$), but time had little effect on them ($P = 0.077$). There was no interaction between location and time ($P = 0.064$). Figure 2 shows that the ADC values at all sites decreased for 3 h post SCI, followed by an increase at the sites of injury epicenter and caudal to it. Almost all the points remained relatively stable for 24 h post-surgery. The values at sites 5, 6, and 7 decreased at 6 weeks postoperatively, whereas the trend at site 4 showed a rise. Sites rostral to the injury point decreased from the beginning of surgery until 24 h, followed by an overall upward trend.

The FA values at different sites were almost similar at precontusion. As shown in Figure 2, almost all the FA values of sites

declined post-injury, gradually increasing after 3 h until 24 h, followed by a 6-week decline after surgery. Site 4 showed a downward trend after surgery until 12 weeks. The mixed-effects modeling analysis showed that site location ($P < 0.001$) and time ($P = 0.002$) influenced FA values significantly. There was no interaction between location and time ($P = 0.309$).

In Figure 2, we see the regularity of MD curve was similar to that of the ADC values. The mixed-effects modeling analysis showed that the site location influenced MD parameters significantly ($P < 0.001$), but time had no effect on them ($P = 0.479$). There was no interaction between location and time ($P = 0.396$). However, interestingly, the value of site 4 at 12 weeks was greater than the normal one. Coincidentally, similar curve regularity was observed in RD parameters. The mixed-effects modeling analysis showed that site location influenced RD values significantly ($P < 0.001$) and time also influenced RD values significantly ($P = 0.046$). There was no interaction between location and time ($P = 0.721$). The description of the parameters values was shown in Table 2. The fixed effects results of mixed effects model were shown in Table 3. The estimates of fixed affects and random effects were described in Table 4.

TABLE 3 The fixed effects results of mixed effects model

DTI Source	F	df	t	n	Sig.
ADC Intercept	241.351	236.471	15.535	7	<0.001
Site	151.795	236.471	12.321	7	<0.001
Time	3.158	242.846	−1.777	7	0.077
site * time	3.451	353.074	−1.858	7	0.064
FA Intercept	896.541	32.539	29.942	7	<0.001
Site	20.478	235.528	−4.525	7	<0.001
Time	15.649	12.681	−3.956	7	0.002
site * time	1.040	235.000	−1.02	7	0.309
MD Intercept	131.022	288.732	11.446	7	<0.001
Site	104.843	288.732	10.239	7	<0.001
Time	0.503	133.964	0.71	7	0.479
site * time	0.722	295.052	−0.85	7	0.396
RD Intercept	66.682	255.271	8.166	7	<0.001
Site	65.237	255.271	8.077	7	<0.001
Time	4.044	140.168	2.011	7	0.046
site * time	0.128	260.740	−0.357	7	0.721

TABLE 4 The estimates of fixed effects and random effects

DTI Effects	Estimated coefficient	Std. Error	95% Confidence Interval Lower bound	Upper bound
ADC Fixed Effects				
Intercept	0.001398##	0.000090	0.001220	0.001575
Site	0.000180##	0.000015	0.000151	0.000209
time	−0.000040	0.000022	−0.000083	0.000004
site * time	−0.000019	0.000010	−0.000039	0.000001
Random Effects				
site	0.000000	0.000000	0.000000	0.000000
time	0.000000	0.000000	0.000000	0.006429
FA Fixed Effects				
Intercept	0.625138##	0.020878	0.582639	0.667638
site	−0.014936##	0.003301	−0.021439	−0.008434
time	-0.019851#	0.005018	−0.030719	−0.008983
site * time	-0.002381	0.002335	−0.006981	0.002218
Random Effects				
site	0.000000	0.000000	0.000000	0.00000
time	0.000023	0.000073	0.000000	0.011307
MD Fixed Effects				
Intercept	0.000821##	0.000072	0.000680	0.000962
site	0.000119##	0.000012	0.000096	0.000142
time	0.000015	0.000021	−0.000027	0.000056
site * time	−0.000007	0.000008	−0.000023	0.000009
Random Effects				
site	0.000000	0.000000	0.000000	0.000000
time	0.000000	0.000000	0.000000	0.000000
RD Fixed Effects				
Intercept	0.000548##	0.000067	0.000416	0.000680
site	0.000088##	0.000011	0.000066	0.000109
time	0.000038#	0.000019	0.000001	0.000076
site * time	−0.000003	0.000008	−0.000018	0.000012
Random Effects				
site	0.000000	0.000000	0.000000	0.000000
time	0.000000	0.000000	0.000000	0.000000

#$P < 0.05$, ##$P < 0.001$
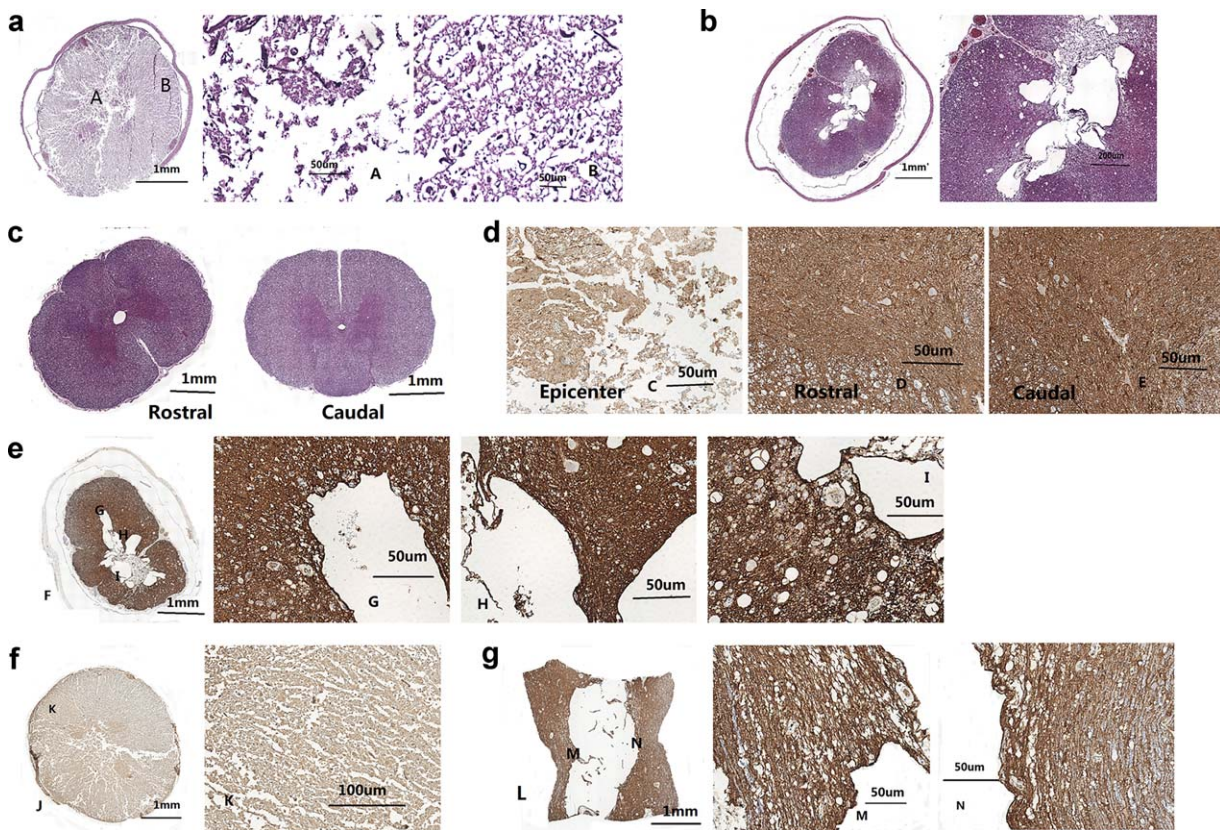
FIGURE 3 (a) HE-stained section showing the spinal cord lesion with extensive parenchymal hemorrhage, necrosis, and edema and loss of normal morphological characteristics on day one following SCI. (b) At 3 months post-injury, the diameter of spinal cord lesion was reduced, and the spine center presented an amorphous cavity. A glial scar surrounding the cyst had a density and color distinct from that of the other tissues. The scattered small vacuoles interspersed the whole cord. (c) HE staining revealed the absence of injury-related histological changes in 1-cm sections rostral and caudal to lesion epicenter. (d) GFAP staining on day 1 post-contusion revealed swelling, degeneration, disordered configuration, and nuclear enlargement of a wide range of astrocytes at the lesion epicenter and both rostral and caudal levels. (e) Reactive astrogliosis at 3 months post-SCI manifesting as hypertrophy and hyperplasia of astrocytes, glial fiber and glial scar formation including a darker pyknotic glial scar surrounding the periphery of lesion cavity. (f) NF staining revealed Wallerian degeneration and abnormal meshwork formation of axon day one following SCI. (g) Regeneration of axons with abnormal orientation at 3 months after injury and growth into the wall cavity, observed especially in the longitudinal sections. [Color figure can be viewed at wileyonlinelibrary.com]

3.3 | Histopathology

Histological and immunohistochemical analysis of the spinal cords postmortem confirmed the DTI observations in the canine models. One of the dogs died on day one post-injury, and was examined under a Tissue FAXS viewer. We found that the HE-stained sections of spinal cord lesion showed extensive parenchymal hemorrhage, necrosis, and edema, as well as loss of normal morphological characteristics on day 1 following SCI (Figure 3A). At 3 months post-injury (Figure 3B), the diameter of spinal cord lesion decreased and the dorsoventral diameter was more prominent than the transverse diameter. An amorphous cavity can be seen at the center of spinal cord, inundated with honeycomb-like trabeculae. A glial scar surrounded the cyst, with a density and color distinct from that of the other tissue and the scattered small vacuoles interspersed in the whole spinal cord. HE staining failed to reveal similar histological changes in the 1-cm sections rostral and caudal to the lesion epicenter (Figure 3C). GFAP staining on day 1 post-contusion revealed extensive swelling, degeneration, and disordered arrangement of astrocytes, as well as enlarged nuclei at the

lesion epicenter and both rostral and caudal sections of the spinal cord (Figure 3D). Reactive astrogliosis was observed at 3 months post-SCI manifesting as astrocyte hypertrophy and hyperplasia, glial fiber formation, and emergence of glial scar. A darker pyknotic glial scar surrounding the periphery of lesion cavity was also observed (Figure 3E). NF staining showed Wallerian degeneration and disordered meshwork of the axons on day one following SCI (Figure 3F). At 3 months after injury, regeneration of a large number of axons with anomalous orientation, including a few that grew into the vicinity of the cavity wall (especially on the longitudinal sections), was observed (Figure 3G). However, fewer axons were found in the glial scar and none in the cavity.

4 | DISCUSSION

We established a canine model of spinal cord contusion and monitored the dynamic changes in DTI parameters of the whole spinal cord from the lesion epicenter to the rostral and caudal levels over an extended

duration post SCI. The study demonstrated that DTI was a sensitive and noninvasive imaging modality to assess the spinal cord structure in dogs. The acute and primary effects of injury were studied in terms of changes in ADC, FA, MD and RD values following spinal cord contusion. The effects varied across the whole spinal cord. The relative changes in diffusivity along the length of the spinal cord were almost consistent with those reported previously (Jirjis, Kurpad, & Schmit, 2013; Lin, He, Schifitto, & Zhong, 2016). The changes in diffusivity were attributed to evolution in vasogenic and cytotoxic edema; hemorrhage; cavity formation; axon and myelin structure damage; and reconstruction, inflammation, and variation in white and gray matter along the length of spinal cord, based on histological and immunohistochemical analyses.

4.1 | Diffusivity parameters reflect documented histological variation in the whole spinal cord

Microstructural damage of the spinal cord tissue might be the primary phenomenon following spinal cord contusion accompanied with vasogenic and cytotoxic edema and hemorrhage resulting in diffusivity variance. Cytotoxic edema is characterized by an increase in intracellular sodium and water leading to cellular swelling with decreased interstitial space (Spatz, 2010). Vasogenic edema is characterized by dissociated neuronal fibers with enlarged interfiber and extracellular spaces (F. Zhao et al., 2006).

Our results suggested a significant decrease in epicenter FA following SCI. The results are consistent with the data reported by Patel et al., which showed that the average slice FA at the injury epicenter at all the four time-points was significantly lower compared with pre-injury levels in a rodent model (Patel et al., 2016). MRI studies in rats ex vivo indicated that FA decreased in both white matter and gray matter after 11 weeks and 24 weeks following SCI, especially at the injury epicenter (Ellingson et al., 2008; Jirjis et al., 2013). C. Zhao et al. (C. Zhao et al., 2016) reported longitudinal variation in FA values at the epicenter and the rostral/caudal levels of the injured spinal cord in rats, and found differentially altered patterns at injury sites. At the epicenter, an obvious decrease in FA occurred only on day one after SCI. At the rostral/caudal levels, however, a drastic decrease in FA occurred on day 3 after SCI. The FA at the epicenter and the rostral/caudal levels was stable by day 7, post SCI, and increased slowly with time. Based on previous studies involving rodents, long-term DTI was performed up to 12 weeks following spinal cord contusion to explore the dynamic changes. As the mechanism of SCI in dogs resembled that of humans, the findings in the animals were extrapolated to conditions in humans. Our results indicated that the changes in FA curve values varied in regions caudal to the lesion epicenter. Rostral levels from lesion epicenter showed an almost up-down trend, while the caudal levels showed a down-up-down trend. These tendencies suggested a significant rostral–caudal asymmetry. Similar asymmetry was also reported in an ex vivo study by Ellingson et al. (2008) and in an in vivo DTI study by Deo et al. (2006).

Substantial decrease in ADC values was observed at all rostral-caudal levels along the length of the spinal cord. The ADC values at the injury and the caudal sites increased at 24 h following contusion inversely and the final values were lower than pre-injury levels. Similar findings were reported by Ellingson et al. (2008), which suggests a significant decrease in longitudinal apparent diffusion coefficient (lADC) in regions away from the lesion epicenter during recovery, and significant increase in transverse apparent diffusion coefficient (tADC) around the lesion epicenter and in fiber bundle, throughout recovery. Wang et al. (2015) suggested that the mean ADC value increased and peaked at 10 weeks after SCI in monkeys, with an abnormal volume occurring at approximately 2 weeks, and peaking at 10 weeks, after contusion. Our results showed a peak at week 12. Analysis of MD and RD values for each site throughout the length of the spinal cord showed trends similar to those observed in ADC over time. Significantly, the changes in RD curve were more prominent. Dalun Leong et al. (2015) studied the correlation between values of RD, ADC, and FA across three normal canine brains and found that the RD values were significantly and robustly correlated with ADC values, while the FA and ADC were not. These findings were almost consistent with our results.

The strong correlation of ADC and RD suggests similar histological findings. The ADC values were indicative of the cellular density. The ADC results appeared to suggest that axonal injury and demyelination occurred throughout the spinal cord as a result of traumatic contusion, and entail changes in axonal (or neurofilament) density and diameter caused by cellular swelling. Axonal damage may occur earlier than myelin damage after contusive injury (Ellingson et al., 2008). MacDonald et al. (2007) showed that the pathological changes in the acute stage were dominated by pure axonal injury, which was caused by disrupted neural filaments and accumulated organelles (Gorrie, Oakes, Duflou, Blumbergs, & Waite, 2002; Maxwell, Domleo, McColl, Jafari, & Graham, 2003; Povlishock, 1993). The injury hindered water diffusion along the axons. In addition, microstructural damage is often associated with cellular and vasogenic edema, which further complicated the interpretation of changes in DTI parameters. In the subacute stage, demyelination was a prominent pathological change that was expected to reduce barriers to diffusion perpendicular to the fiber direction (Mac Donald et al., 2007; Song et al., 2005). Lin et al. (2016) used Monte Carlo simulations to explore changes in DTI metrics at different time points after TBI. FA, MD, and RD were calculated based on the diffusion tensor model. Simulation of DTI parameters was associated with tissue pathology following axonal injury occurring via reduced diffusivity. By contrast, vasogenic edema increased the separation between axons, while cytotoxic edema increased glial cell diameter. Demyelination occurred by increasing the myelin sheath permeability, which affected DTI parameters via tortuosity. The simulation was validated using clinical and animal models. In TBI, the DTI results were more variable. Three distinctive patterns of diffusion abnormalities have been reported: type 1, reduced FA and reduced or unchanged MD (Arfanakis et al., 2002; Huisman et al., 2004); type 2, elevated FA and reduced MD (Bazarian et al., 2007; Mayer et al., 2010; Wilde et al., 2008); and type 3, reduced FA and elevated MD (Miles et al., 2008; Rutgers et al., 2008). Similar changes might occur in spinal cord injury due to similar microstructure. Axonal injury played a dominant role in the acute

stages leading to pattern one of the altered DTI parameters, including reduced FA, reduced or unchanged MD, and reduced RD. Vasogenic and cytotoxic edema can coexist and may originate in the accumulated tissue, but have contrasting effects on DTI parameters. Vasogenic edema alone leads to type 3 pattern involving a combination of reduced FA, elevated MD, and elevated RD. Conversely, cytotoxic edema is more likely to lead to type 2 pattern, characterized by elevated FA and reduced MD and elevated RD. Demyelination often occurred in the subacute stages, resulting in a significant reduction of FA and elevation of MD and RD. Notably, vasogenic and cytotoxic edema may also coexist, leading to contrasting effects on DTI parameters. However, they contribute simultaneously to the DTI signal, and therefore, cancel out the opposing effects. In addition, white matter is inherently more anisotropic than gray matter, and these changes were probably due to the lower white-to-gray matter ratio in more caudal segments (Patel et al., 2016). Therefore, distance plays an important role in altered DTI parameters. Lin et al. (2016) reported that DTI measurements are also affected by physical properties of tissues including the size and shape of cells and the intercellular space, as well as the permeability of cell membranes. Proteins, amines, amides, and hydroxyl groups also mediate the progression of lesion after spinal cord injury, which might affect the DTI results (Wang et al., 2015). The pathological changes might have altered the DTI parameter curves of the spinal cord in our study.

4.2 | Diffusivity parameters reflect documented histological variations in gray matter

Changes in GM diffusivity may be attributed to the differences in the composition and structure of spinal cord. Histopathology and immunohistochemistry revealed that cavity formation mainly occurred in gray matter, especially in the injured region. However, we found no cavity in the rostral and caudal levels away from epicenter. Further, the astrocytic activity in GM triggered by Wallerian degeneration in WM may also contribute to the changes partially (Buss et al., 2004; Ellingson, Schmit, & Kurpad, 2010). The rudimentary cavity developed at 2 weeks post-injury. A large cyst filled with an amorphous substance and liquid surrounded by a glial scar was observed at 4 weeks after the injury (Hu et al., 2010). Trabeculae were found inside the cavity. Wang et al (2015) defined cyst formation as onset (2 week post SCI), followed by increased ADC value, which peaked at about 10 weeks, at leats partially consistent with our results. To our knowledge, a limited number of studies have reported diffusion characteristics from the GM regions; our study provides additional information in this aspect.

4.3 | Histopathology

Immunohistological analysis of GFAP and NF following the terminal MRI imaging revealed pathologic changes associated with reactive astrocytes and axons, as well as the cavity and glial scars formed during the chronic stages of SCI. All these changes provide relative evidence underlying the DTI parameters. Hu et al (2010) reported that the injured axons showed potential for regrowth, which might contribute

to spontaneous recovery after SCI. Our results suggest regeneration of large numbers of anomalously oriented axons. A few of these axons grow into the vicinity of the cavity wall (especially on the longitudinal sections) at 3 months after injury. However, fewer axons appeared in the glial scar and none in the cavity, which suggested that the glial scar acted as a barrier against axon extension. Intermediate flaments such as GFAP and vimentin (a hallmark of reactive astrocytes) are upregulated after SCI, which was consistent with our findings. Silencing the expression of these filaments reduces glial scar formation and promotes axonal regeneration after CNS injury (Menet et al., 2003; Wilhelmsson et al., 2004).

4.4 | Study limitation

The study limitations are as follows. First, although we designed the large animal SCI model impactor and applied for the patent, the study still represents preliminary findings. Further data are necessary to corroborate the results. Second, the sample size was small, but the sampling error was large. However, further studies will be carried out with increased sample size and further differentiated degrees of SCI. Third, since the animals are under anesthesia, the respiratory and heart rates affect the acquisition of MRI signals. Fourth, the low spatial resolution of DTI was also a limitation and partial volume effects influenced our results. Lastly, the sex of the sample may be a biological variable, the potential sex differences will be explored, and we hope to conduct scoring and analysis of the correlation between behavior and DTI parameters in the future.

5 | CONCLUSIONS

Our study established a canine model of spinal cord contusion and determined the dynamic changes in DTI parameters of the whole spinal cord post SCI. We further demonstrated that DTI was a sensitive and noninvasive imaging tool to assess edema, hemorrhage, cavity formation, axon and myelin structure damage and reconstruction, and spinal cord inflammation in dogs. The regularity of different DTI parameters after contusion varied; however, the trend of ADC, MD, and RD curves was nearly similar and the FA was distinct. All the DTI parameters were affected by distance and time. Although our study is preliminary, our results offer an experimental basis for fundamental and clinical research. Our canine model is translational and facilitates investigation into human spinal cord pathology.

CONFLICT OF INTEREST

The authors declare that they have no potential conflicts of interest, including financial, personal, or other relationships that could inappropriately influence or be perceived to influence the work presented here.

AUTHOR CONTRIBUTIONS

Conceptualization: Jianjun Li and Degang Yang, Mingliang Yang, Changbin Liu; Methodology: Degang Yang, Mingliang Yang, Changbin Liu, Zhentao Zuo, Dapeng Li, Liangjie Du, Rui GU, Wei Sun, Jun Li, Qi Miao and Feng Gao; MRI measurement and post-processing: Zhentao Zuo and Changbin Liu; Statistical Analysis: Changbin Liu, Xuechao Dong, Xinghua Yang; Animal caring: Changbin Liu, Qianru Meng, Wenhao Zhang, Chang Cai, Yutong Feng; Writing: Changbin Liu, Degang Yang, Zhentao Zuo.

ORCID

Changbin Liu (iD) http://orcid.org/0000-0002-3564-8654

REFERENCES/WORKS CITED

Ackery, A., Tator, C., & Krassioukov, A. (2004). A global perspective on spinal cord injury epidemiology. *Journal of Neurotrauma, 21*:1355–1370.

Arfanakis, K., Haughton, V. M., Carew, J. D., Rogers, B. P., Dempsey, R. J., & Meyerand, M. E. (2002). Diffusion tensor MR imaging in diffuse axonal injury. *American Journal of Neuroradiology, 23*:794–802.

Basser, P. J., Mattiello, J., & LeBihan, D. (1994). MR diffusion tensor spectroscopy and imaging. *Biophysical Journal, 66*:259–267.

Bazarian, J. J., Zhong, J., Blyth, B., Zhu, T., Kavcic, V., & Peterson, D. (2007). Diffusion tensor imaging detects clinically important axonal damage after mild traumatic brain injury: a pilot study. *Journal of Neurotrauma, 24*:1447–1459.

Boekhoff, T. M., Flieshardt, C., Ensinger, E. M., Fork, M., Kramer, S., & Tipold, A. (2012). Quantitative magnetic resonance imaging characteristics: evaluation of prognostic value in the dog as a translational model for spinal cord injury. *Journal of Spinal Disorders & Techniques, 25*:E81–87.

Buss, A., Brook, G. A., Kakulas, B., Martin, D., Franzen, R., Schoenen, J., . . . Schmitt, A. B. (2004). Gradual loss of myelin and formation of an astrocytic scar during Wallerian degeneration in the human spinal cord. *Brain. 127*:34–44.

Chiu, W. T., Lin, H. C., Lam, C., Chu, S. F., Chiang, Y. H., & Tsai, S. H. (2010). Review paper: epidemiology of traumatic spinal cord injury: comparisons between developed and developing countries. *Asia Pacific Journal of Public Health, 22*:9–18.

Deo, A. A., Grill, R. J., Hasan, K. M., & Narayana, P. A. (2006). In vivo serial diffusion tensor imaging of experimental spinal cord injury. *Journal of Neuroscience Research, 83*:801–810.

Dong, X., Yang, D., Li, J., Liu, C., Yang, M., Du, L., . . . Zhang, H. (2016). Intramedullary pressure changes in rats after spinal cord injury. *Spinal Cord 54*:947–950.

Ellingson, B. M., Kurpad, S. N., & Schmit, B. D. (2008). Ex vivo diffusion tensor imaging and quantitative tractography of the rat spinal cord during long-term recovery from moderate spinal contusion. *Journal of Magnetic Resonance Imaging, 28*:1068–1079.

Ellingson, B. M., Schmit, B. D., & Kurpad, S. N. (2010). Lesion growth and degeneration patterns measured using diffusion tensor 9.4-T magnetic resonance imaging in rat spinal cord injury. *Journal of Neurosurgery: Spine, 13*:181–192.

Fukuda, S., Nakamura, T., Kishigami, Y., Endo, K., Azuma, T., Fujikawa, T., . . . Shimizu, Y. (2005). New canine spinal cord injury model free from laminectomy. *Brain Research. Brain Research Protocols, 14*:171–180.

Gorrie, C., Oakes, S., Duflou, J., Blumbergs, P., & Waite, P. M. (2002). Axonal injury in children after motor vehicle crashes: extent, distribution, and size of axonal swellings using beta-APP immunohistochemistry. *Journal of Neurotrauma, 19*:1171–1182.

Grace, C. E., Schaefer, T. L., Herring, N. R., Graham, D. L., Skelton, M. R., Gudelsky, G. A., . . . Vorhees, C. V. (2010). Effect of a neurotoxic dose regimen of (+)–methamphetamine on behavior, plasma corticosterone, and brain monoamines in adult C57BL/6 mice. *Neurotoxicology and Teratology, 32*:346–355.

Hobert, M. K., Stein, V. M., Dziallas, P., Ludwig, D. C., & Tipold, A. (2013). Evaluation of normal appearing spinal cord by diffusion tensor imaging, fiber tracking, fractional anisotropy, and apparent diffusion coefficient measurement in 13 dogs. *Acta Veterinaria Scandinavica, 55*:36.

Hu, R., Zhou, J., Luo, C., Lin, J., Wang, X., Li, X., . . . Feng, H. (2010). Glial scar and neuroregeneration: histological, functional, and magnetic resonance imaging analysis in chronic spinal cord injury. *Journal of Neurosurgery: Spine, 13*:169–180.

Huisman, T. A., Schwamm, L. H., Schaefer, P. W., Koroshetz, W. J., Shetty-Alva, N., Ozsunar, Y., . . . Sorensen, A. G. (2004). Diffusion tensor imaging as potential biomarker of white matter injury in diffuse axonal injury. *American Journal of Neuroradiology, 25*:370–376.

Jeffery, N. D., Smith, P. M., Lakatos, A., Ibanez, C., Ito, D., & Franklin, R. J. (2006). Clinical canine spinal cord injury provides an opportunity to examine the issues in translating laboratory techniques into practical therapy. *Spinal Cord, 44*:584–593.

Jirjis, M. B., Kurpad, S. N., & Schmit, B. D. (2013). Ex vivo diffusion tensor imaging of spinal cord injury in rats of varying degrees of severity. *Journal of Neurotrauma, 30*:1577–1586.

Khan, M., & Griebel, R. (1983). Acute spinal cord injury in the rat: comparison of three experimental techniques. *Canadian Journal of Neurological Sciences, 10*:161–165.

Kulkarni, M. V., McArdle, C. B., Kopanicky, D., Miner, M., Cotler, H. B., Lee, K. F., & Harris, J. H. (1987). Acute spinal cord injury: MR imaging at 1.5 T. *Radiology, 164*:837–843.

Lee, J. W., Kim, J. H., Park, J. B., Park, K. W., Yeom, J. S., Lee, G. Y., & Kang, H. S. (2011). Diffusion tensor imaging and fiber tractography in cervical compressive myelopathy: preliminary results. *Skeletal Radiology, 40*:1543–1551.

Leong, D., Calabrese, E., White, L. E., Wei, P., Chen, S., Platt, S. R., & Provenzale, J. M. (2015). Correlation of diffusion tensor imaging parameters in the canine brain. *The Neuroradiology Journal, 28*:12–18.

Lin, M., He, H., Schifitto, G., & Zhong, J. (2016). Simulation of changes in diffusion related to different pathologies at cellular level after traumatic brain injury. *Magnetic Resonance in Medicine, 76*:290–300.

Loy, D. N., Kim, J. H., Xie, M., Schmidt, R. E., Trinkaus, K., & Song, S. K. (2007). Diffusion tensor imaging predicts hyperacute spinal cord injury severity. *Journal of Neurotrauma, 24*:979–990.

Mac Donald, C. L., Dikranian, K., Bayly, P., Holtzman, D., & Brody, D. (2007). Diffusion tensor imaging reliably detects experimental

traumatic axonal injury and indicates approximate time of injury. *Journal of Neuroscience*, 27:11869–11876.

Martin, A. R., Aleksanderek, I., Cohen-Adad, J., Tarmohamed, Z., Tetreault, L., Smith, N., ... Fehlings, M. G. (2016). Translating state-of-the-art spinal cord MRI techniques to clinical use: A systematic review of clinical studies utilizing DTI, MT, MWF, MRS, and fMRI. *NeuroImage: Clinical*, 10:192–238.

Maxwell, W. L., Domleo, A., McColl, G., Jafari, S. S., & Graham, D. I. (2003). Post-acute alterations in the axonal cytoskeleton after traumatic axonal injury. *Journal of Neurotrauma*, 20:151–168.

Mayer, A. R., Ling, J., Mannell, M. V., Gasparovic, C., Phillips, J. P., Doezema, D., ... Yeo, R. A. (2010). A prospective diffusion tensor imaging study in mild traumatic brain injury. *Neurology*, 74:643–650.

Menet, V., Prieto, M., Privat, A., Gimenez, Y., & Ribotta, M. (2003). Axonal plasticity and functional recovery after spinal cord injury in mice deficient in both glial fibrillary acidic protein and vimentin genes. *Proceedings of the National Academy of Sciences U S A, 100*: 8999–9004.

Miles, L., Grossman, R. I., Johnson, G., Babb, J. S., Diller, L., & Inglese, M. (2008). Short-term DTI predictors of cognitive dysfunction in mild traumatic brain injury. *Brain Injury*, 22:115–122.

Onose, G., Anghelescu, A., Muresanu, D. F., Padure, L., Haras, M. A., Chendreanu, C. O., ... von Wild, K. R. (2009). A review of published reports on neuroprotection in spinal cord injury. *Spinal Cord*, 47:716–726.

Patel, S. P., Smith, T. D., VanRooyen, J. L., Powell, D., Cox, D. H., Sullivan, P. G., & Rabchevsky, A. G. (2016). Serial diffusion tensor imaging in vivo predicts long-term functional recovery and histopathology in rats following different severities of spinal cord injury. *Journal of Neurotrauma*, 33:917–928.

Povlishock, J. T. (1993). Pathobiology of traumatically induced axonal injury in animals and man. *Annals of Emergency Medicine*, 22:980–986.

Purdy, P. D., White, C. L., Baer, D. L., Frawley, W. H., Reichard, R. R., Pride, G. L., ... Yetkin Z. (2004). Percutaneous translumbar spinal cord compression injury in dogs from an angioplasty balloon: MR and histopathologic changes with balloon sizes and compression times. *American Journal of Neuroradiology*, 25:1435–1442.

Rabchevsky, A. G., Fugaccia, I., Sullivan, P. G., Blades, D. A., & Scheff, S. W. (2002). Efficacy of methylprednisolone therapy for the injured rat spinal cord. *Journal of Neuroscience Research*, 68:7–18.

Rutgers, D. R., Fillard, P., Paradot, G., Tadie, M., Lasjaunias, P., & Ducreux, D. (2008). Diffusion tensor imaging characteristics of the corpus callosum in mild, moderate, and severe traumatic brain injury. *American Journal of Neuroradiology*, 29:1730–1735.

Song, S. K., Yoshino, J., Le, T. Q., Lin, S. J., Sun, S. W., Cross, A. H., & Armstrong, R. C. (2005). Demyelination increases radial diffusivity in corpus callosum of mouse brain. *Neuroimage*, 26:132–140.

Spatz, M. (2010). Past and recent BBB studies with particular emphasis on changes in ischemic brain edema: dedicated to the memory of Dr. Igor Klatzo. *Acta Neurochirurgica Supplement*, 106:21–27.

Tay, B., Hyun, J. K., & Oh, S. (2014). A machine learning approach for specification of spinal cord injuries using fractional anisotropy values obtained from diffusion tensor images. *Computational and Mathematical Methods in Medicine*, 2014:276589.

Wang, F., Huang, S. L., He, X. J., & Li, X. H. (2014). Determination of the ideal rat model for spinal cord injury by diffusion tensor imaging. *Neuroreport*, 25:1386–1392.

Wang, F., Qi, H. X., Zu, Z., Mishra, A., Tang, C., Gore, J. C., & Chen, L. M. (2015). Multiparametric MRI reveals dynamic changes in molecular signatures of injured spinal cord in monkeys. *Magnetic Resonance in Medicine*, 74:1125–1137.

Webb, A. A., Ngan, S., & Fowler, D. (2010). Spinal cord injury II: Prognostic indicators, standards of care, and clinical trials. *The Canadian Veterinary Journal*, 51:598–604.

Wilde, E. A., McCauley, S. R., Hunter, J. V., Bigler, E. D., Chu, Z., Wang, Z. J., ... Levin, H. S. (2008). Diffusion tensor imaging of acute mild traumatic brain injury in adolescents. *Neurology*, 70:948–955.

Wilhelmsson, U., Li, L., Pekna, M., Berthold, C. H., Blom, S., Eliasson, C., Renner O, ... Pekny, M. (2004). Absence of glial fibrillary acidic protein and vimentin prevents hypertrophy of astrocytic processes and improves post-traumatic regeneration. *Journal of Neuroscience, 24*: 5016–5021.

Xiangshui, M., Xiangjun, C., Xiaoming, Z., Qingshi, Z., Yi, C., Chuanqiang, Q., ... Jinwen, H. (2010). 3 T magnetic resonance diffusion tensor imaging and fibre tracking in cervical myelopathy. *Clinical Radiology*, 65:465–473.

Xu, J. C., Bernreuther, C., Cui, Y. F., Jakovcevski, I., Hargus, G., Xiao, M. F., & Schachner, M. (2011). Transplanted L1 expressing radial glia and astrocytes enhance recovery after spinal cord injury. *Journal of Neurotrauma*, 28:1921–1937.

Young, W. (2002). Spinal cord contusion models. *Progress in Brain Research*, 137:231–255.

Zhao, C., Rao, J. S., Pei, X. J., Lei, J. F., Wang, Z. J., Yang, Z. Y., & Li, X. G. (2016). Longitudinal study on diffusion tensor imaging and diffusion tensor tractography following spinal cord contusion injury in rats. *Neuroradiology*, 58:607–614.

Zhao, F. Y., Kuroiwa, T., Miyasakai, N., Tanabe, F., Nagaoka, T., Akimoto, H., ... Tamura, A. (2006). Diffusion tensor feature in vasogenic brain edema in cats. *Acta Neurochirurgica Supplement*, 96:168–170.